Ultrasound in Medicine & Biology 50 (2024) 860–868

Contents lists available at ScienceDirect

Ultrasound in Medicine & Biology

journal homepage: www.elsevier.com/locate/ultrasmedbio

Original Contribution

Patient-Specific Vascular Flow Phantom for MRI- and Doppler Ultrasound Imaging

Sadaf Soloukey [a,b,†,*], Bastian Generowicz [a,†], Esther Warnert [c,d], Geert Springeling [e], Joost Schouten [b], Chris De Zeeuw [a,f], Clemens Dirven [b], Arnaud Vincent [b], Pieter Kruizinga [a]

[a] Department of Neuroscience, Erasmus MC, Rotterdam, The Netherlands
[b] Department of Neurosurgery, Erasmus MC, Rotterdam, The Netherlands
[c] Deparment of Radiology and Nuclear Medicine, Erasmus MC, Rotterdam, The Netherlands
[d] Erasmus MC Cancer Institute, Rotterdam, The Netherlands
[e] Deparment of Experimental Medical Instrumentation, Erasmus MC, Rotterdam, The Netherlands
[f] Netherlands Institute for Neuroscience, Royal Dutch Academy for Arts and Sciences, Amsterdam, Netherlands

ARTICLE INFO

Keywords:
Flow phantom
Multimodal
MRI
Wall-less
Water-soluble
Resin
Patient-specific
Cerebral vasculature

ABSTRACT

Objective: Intraoperative Doppler ultrasound imaging of human brain vasculature is an emerging neuro-imaging modality that offers vascular brain mapping with unprecedented spatiotemporal resolution. At present, however, access to the human brain using Doppler Ultrasound is only possible in this intraoperative context, posing a significant challenge for validation of imaging techniques. This challenge necessitates the development of realistic flow phantoms *outside* of the neurosurgical operating room as external platforms for testing hardware and software. An ideal ultrasound flow phantom should provide reference-like values in standardized topologies such as a slanted pipe, and allow for measurements in structures closely resembling vascular morphology of actual patients. Additionally, the phantom should be compatible with other clinical cerebrovascular imaging modalities. To meet these criteria, we developed and validated a versatile, multimodal MRI- and ultrasound Doppler phantom.

Methods: Our approach incorporates the latest advancements in phantom research using tissue-mimicking material and 3D-printing with water-soluble resin to create wall-less patient-specific lumens, compatible for ultrasound and MRI.

Results: We successfully produced three distinct phantoms: a slanted pipe, a y-shape phantom representing a bifurcating vessel and an arteriovenous malformation (AVM) derived from clinical Digital Subtraction Angiography (DSA)-data of the brain. We present 3D ultrafast power Doppler imaging results from these phantoms, demonstrating their ability to mimic complex flow patterns as observed in the human brain. Furthermore, we showcase the compatibility of our phantom with Magnetic Resonance Imaging (MRI).

Conclusion: We developed an MRI- and Doppler Ultrasound-compatible flow-phantom using customizable, water-soluble resin prints ranging from geometrical forms to patient-specific vasculature.

Introduction

Imaging phantoms are an essential tool in diagnostic imaging, facilitating the development and standardized testing of software and hardware for clinical applications. Phantoms are used to study reliability and efficacy of the imaging modality in question and can be specifically designed to simulate in-vivo clinical observations. For the context of Doppler ultrasound-imaging of human brain vasculature, ultrasound phantoms that mimic cerebrovascular flow are especially essential. As the human skull attenuates ultrasound signals, acoustic access to the human brain is often only achievable in the limited intraoperative context. Realistic flow phantoms allow for the development of cerebrovascular flow imaging techniques *outside* of the constraints of the neurosurgical operating room.

In addition to Doppler ultrasound imaging, other techniques such as Digital Substraction Angiography (DSA) [1], Magnetic Resonance Angiography (MRA) [2] or Computed Tomography Angiography (CTA) [3] are also used to image human cerebrovascular flow. In the clinical

Abbreviations: AVM, arteriovenous malformations; CTA, computed tomography angiography; DSA, digital subtraction angiography; dOCT, doppler Optical Coherence Tomography; MRA, magnetic resonance angiography; MRI, magnetic resonance imaging; PDI, power doppler image; RPM, revolutions per minute; SEBS, styrene-ethylene/butylene-styrene; SVD, singular value decomposition

* Corresponding author. Department of Neuroscience and Neurosurgery, Erasmus Medical Center, Rotterdam, The Netherlands.
E-mail address: s.soloukeytbalvandany@erasmusmc.nl (S. Soloukey).
† Both authors contributed equally.

https://doi.org/10.1016/j.ultrasmedbio.2024.02.010
Received 21 October 2023; Revised 29 January 2024; Accepted 16 February 2024

treatment of cerebrovascular disease, these imaging modalities are often combined. For example, in the neurosurgical treatment of arteriovenous malformations (AVMs), preoperative MRA, CTA or DSA are often used to plan the surgical procedure. Intraoperative DSA and Doppler ultrasound are available to monitor the surgical resection. Postoperative MRA, CTA or DSA are used to follow-up treatment efficacy. To ideally reflect the clinical context, a flow phantom should therefore be compatible with multiple of these imaging modalities. In Figure 1 we summarize a set of features of an ideal Doppler ultrasound flow phantom for cerebrovascular imaging.

How do currently available imaging phantoms compare to this ideal flow phantom?

Both experimental and commercial [4] imaging phantoms exist to optimize imaging parameters or practice clinical procedures [5–8]. This class of phantoms is often not patient-specific nor easily customizable. Commercial [9] and experimental phantoms similarly exist for other modalities such as MRI. However, only a subset of these phantoms are compatible with multiple modalities including Doppler Ultrasound [10–12].

More recently, patient-specific vascular phantoms, both with and without vessel walls, have been described by a number of works [13–21]. Wall-less phantoms are advantageous for Doppler Ultrasound in many cases as they avoid unwanted acoustic interference from the wall material. However, many of the wall-less vascular phantoms encountered in literature were not demonstrated in the context of Doppler ultrasound imaging, nor was their compatibility with MRI evaluated. Patient-specific structural phantoms based on MRI/CT have also been described in literature as useful tools for surgical planning [18,22], without incorporating blood flow imaging.

In this manuscript, we aim to develop a multimodal, MRI- and Doppler Ultrasound-compatible flow phantom that realizes all the features described in Figure 1. Specifically, we describe the production of a wall-less, styrene-ethylene/butylene-styrene (SEBS)-based [23], tissue-mimicking ultrasound flow phantom, generating the wall-less vessels using 3D-printing with a water-soluble resin. We showcase results from three specific phantoms fabricated in-house: a slanted pipe, a y-shape phantom representing a simple bifurcating vessel, and an arteriovenous malformation (AVM) segmented from a clinical Digital Subtraction Angiography (DSA) image. Using different flow and injection pumps connected to our custom-made imaging set-up, we demonstrate the ability to image flow in our phantoms using Doppler Ultrasound. We show both 2D-Power Doppler Images (PDIs) as well as 3D-reconstructions generated using a motorized linear stage to stagger multiple stationary 2D-recordings along the phantom volume (*staged-3D*). For this work we focus specifically on Power rather than Color Doppler imaging due to its higher sensitivity to small vessels in the brain [24] and its capability to reveal unique vascular details of human brain tissue [25]. Finally, we demonstrate multimodal properties of the phantoms by imaging them using structural and flow-based MRI.

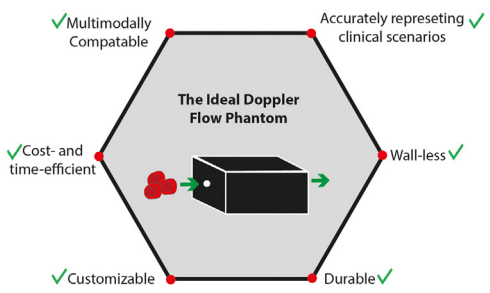

Figure 1. The Ideal Doppler Flow Phantom. Figure representing the ideal set of characteristics for a Doppler Flow phantom.

Materials and methods

Phantom fabrication

Print design

We designed three different prints which we considered to be interesting in the context of Doppler imaging (Fig. 2a):

- #1 - A slanted pipe (representing a simplified, straight single vessel)
- #2 - A y-shape (representing a simplified vascular bifurcation)
- #3 - A cerebrovascular structure derived from a real patient case of an arteriovenous malformation (AVM) in the brain (previously published by our group [26]).

Prints #1 and #2 were designed in Solidworks (Dassault Systèmes SolidWorks Corporation). Print #3 was extracted based on a clinical Digital Subtraction Angiography (DSA) using 3D Slicer [27]. Print #3 was extracted from a clinical Digital Subtraction Angiography (DSA) image using 3D Slicer [27] and subsequently smoothed using the autofiller option within Meshmixer (Autodesk Inc.). Each print design was extended with a fixed-diameter cylinder to allow each print to fit in a custom-designed phantom mold (Fig. 2c).

Phantom mold

Molds were milled from aluminum to stabilize the resin prints during the pouring process. The prints were suspended in the mold using either two (Print #1) or three (Print #2 and #3) aluminum rods, corresponding to in-and outlet tracts (Fig. 2c). The mold was designed to be robust, heat-resistant and allow for consistency across different phantom iterations.

Resin printing

All designs were printed using the Envisiontec Vida HD cDLM resin-printer. The printing material consisted of a commercially available cyan-blue water-soluble resin (3D resyn, IM HDT-WS) (Fig. 3a). Printer settings are summarized Supplementary File 1. After printing, the print was removed from the printing surface, and the support structures were broken off using tweezers (Fig. 3b, c). Next the print was placed in an ultrasonic bath filled with 2-propanolol for 2 rounds of 2-min washing, carefully drying the design between rounds using pressurized air. Finally, the print design was oven-dried at 37°C for 30–60 min, then cured a in a light polymerization chamber (Envisiontec Otoflash) (Fig. 3d).

Phantom pouring

The cured resin print was fixated inside the phantom mold (Fig. 4a). For the tissue-mimicking material, we recreated *'sample A5'* from Cabrelli et al. [23]. The mixture consisted of styrene-ethylene/butylene-styrene (SEBS) in mineral oil (Fig. 4a). Glycerol was added to improve the acoustic impedance of the material, titanium dioxide (TiO_2) was added as a scattering medium. Exact details of the mixture-ratios are presented in Table 1. The powdered TiO_2 was first mixed with the glycerol and subjected to sonification for 5 min, before being added to the mineral oil in a large (1L) beaker. Next, the SEBS powder was mixed into the container, after which it was placed on a heating plate. The mixture was heated until it reached 130°C while stirring intermittently (Fig. 4b). Stirring of the mixture was essential to avoid the TiO_2 sinking to the bottom However, we found that over stirring introduced air bubbles, which made the material less homogeneous and increased its scattering. As such stirring was performed manually and slowly, with a spoon continuously submerged in the mixture to avoid introduction of air bubbles from removing and reinserting the spoon.

Once the material reached the desired temperature of 130°C, the beaker was removed from the hot plate, and slowly stirred until it reached a temperature of 90°C. At this temperature, the mixture's viscosity still allowed for easy pouring while avoiding overheating of the resin

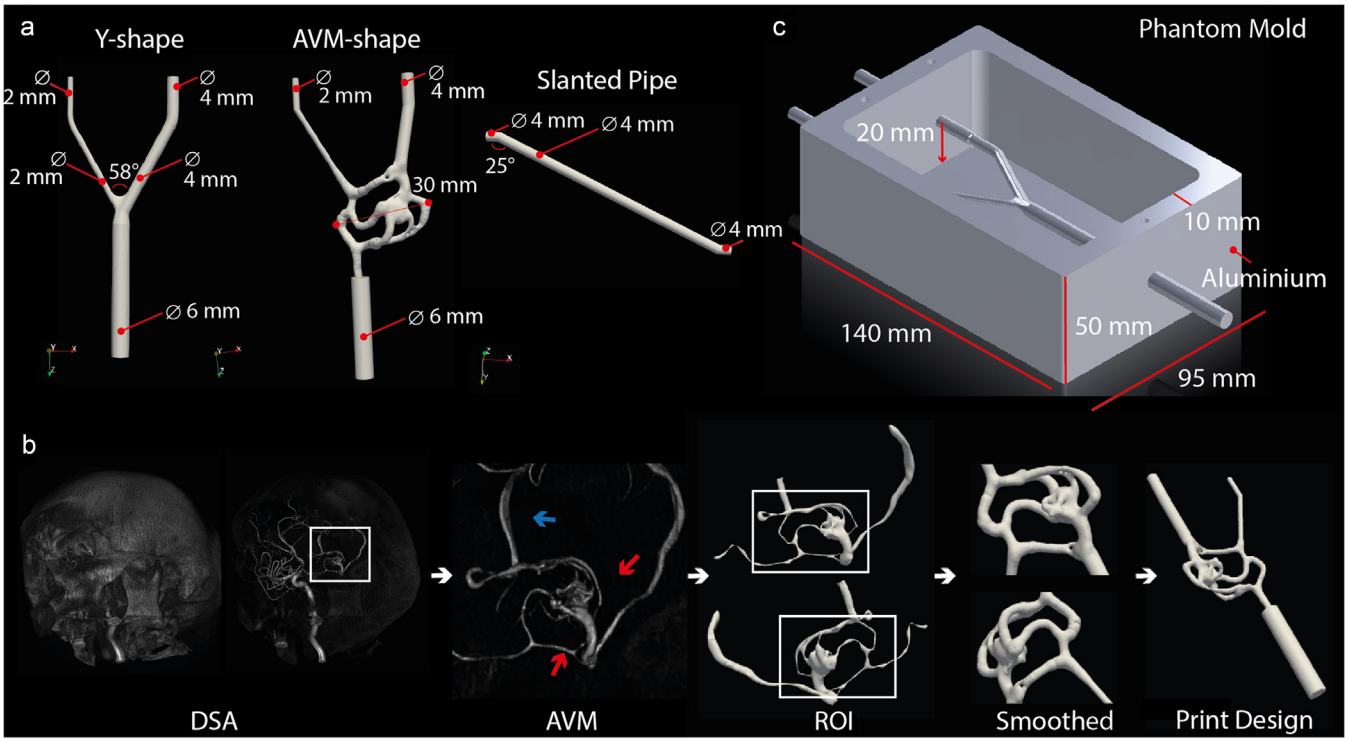

Figure 2. Resin print designs for three Doppler-phantoms. (a) Three print-designs were created for three types of Doppler-phantoms: 1) a horizontal y-shape, representing a simplified vascular bifurcation, 2) an cerebrovascular structure based on a real patient case of an AVM previously published by our group [26] and 3) a slanted pipe representing a simplified, single vessel. Each design was extended with a fixed-diameter cylinder. (b) The fixed cylinders allowed each print to fit in our custom-designed phantom mold depicted here. (c) For the AVM-phantom specifically, the print design was extracted based on a clinical DSA-scan. This relatively small AVM was known to have two major feeding and one major draining vessel [26]. AVM, arteriovenous malformation; DSA, digital substraction angiography.

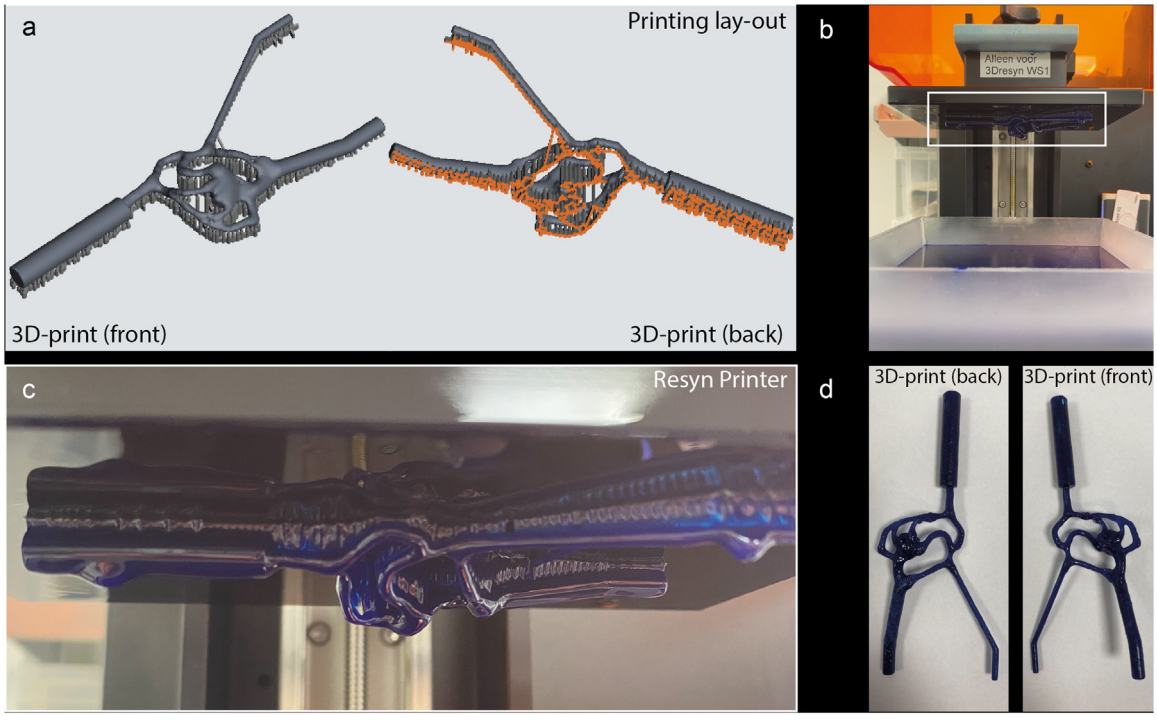

Figure 3. The resin-printing procedure. (a) The AVM-shape printing lay-out including support placement, prepared for printing. (b) All designs were printed using the Envisiontec Vida HD cDLM resin-printer combined with commercially available cyan-blue water-soluble resin-material (3D-resin, IM-HDT-WS). (c) Zoom-in on the finished AVM-shape resin print, still connected to the printing base plate through the support material. (d) Photos of the cleaned and cured AVM-shape printing design.

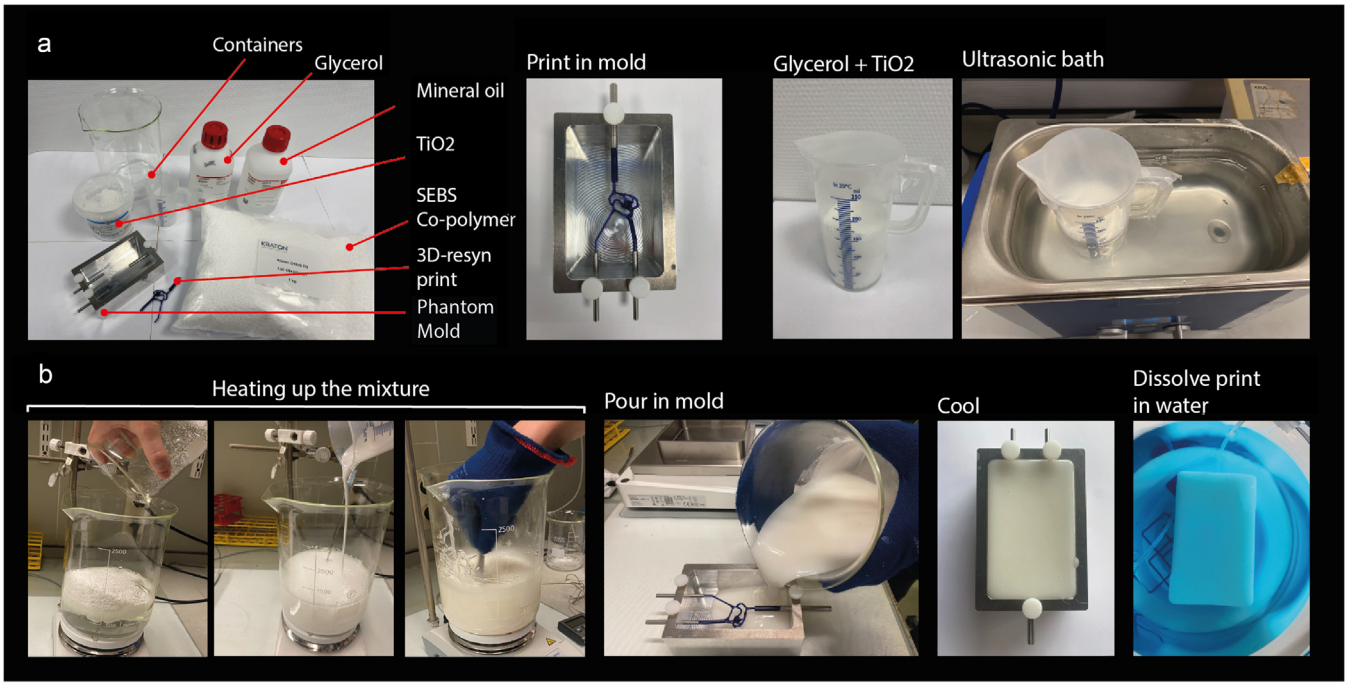

Figure 4. Phantom Pouring Procedure. (a) (1) Overview of necessary supplies and materials for the phantom pouring process, (2) the AVM print placed inside the pouring mold, (3–4) the sonication process for the glycerol + TiO_2 mixture. (b) Overview of the next steps in the pouring process. The mixture was first heated up to 130°C, before being cooled down to 90°C and poured inside the mold. The phantom was then cooled >12 h, before dissolving the encapsulated print in water in <24 h.

print (Fig. 4b). The phantom was cooled for at least 12 h at room temperature then removed from the mold.

Phantom dissolving

After cooling, the phantom was submersed in a water bath and a small, submersible aquarium pump (ICQUANZX, no 01554) was placed in one of the in/out-lets to allow for continuous flow of water inside the phantom accelerating the dissolving process (Fig. 4b). The water inside the bath was periodically refreshed to prevent saturation. Within a period of 24 h, the resin inside the phantom was fully dissolved (see Supplementary Video 1).

Phantom in- and outlets

To prepare the phantom for installation in the imaging unit, connecting tubes (6–7 mm in diameter) were permanently glued to the inside of the first 1 cm of the in- and outflow tracts using cyanoacrylate and silicone glue.

Fabrication time

Overall, the full phantom fabrication process (from resin printing to phantom pouring, cooling, and dissolving) took an average of 2 days.

Phantom imaging

Ultrasound

Imaging setup. To allow for consistent Doppler measurements across different imaging sessions and different phantom iterations, we built a custom tank using PMMA. This featured in and outflow tracts for interfacing with phantoms and an acoustic absorber at the bottom to eliminate reflections (Fig. 5a). The tank could be connected to both syringe (Harvard apparatus, PHD Ultra) and peristaltic (Masterflex L/S) pumps for flow regulation. For each Doppler flow experiment the connecting tubes glued inside each phantom were connected to the tank's in- and outflow tracts (Fig. 5b) and the tubing was filled with Doppler scattering fluid (CIRS, Model 769DF) to provide acoustic contrast.

Data acquisition. All measurements were performed using a 9L-D linear array transducer (GE, 5.3 MHz) driven by an experimental research system (Vantage-256, Verasonics). For each experiment the transducer was mounted above the phantom and coupled to it using ultrasound gel. The probe was driven continuously with a set of 10–12 angled plane waves equally spaced between −12 and 12 degrees. Each set of angled transmissions was coherently compounded to form beamformed frames (BFs) with a PRF of 1 kHz. During most experiments ensembles of 200

Table 1
Details of SEBS-mixture

Material	Quantity used per phantom	Supplier and Catalogue Number
Mineral Oil	900 mL* **600 mL was necessary to fill the phantom mold, but more would be made to avoid pouring the bottom of the container where scatterers would pile up.*	Sigma Aldrich M3516
Styrene-Ethylene/Butylene-Styrene (SEBS)	10% 90 g	Kraton Polymers Research B.V G1650E
Glycerol	15% 135 mL	Sigma Aldrich G9012
TiO_2	0.2% 1.8 g	Keramikos NL CH131D

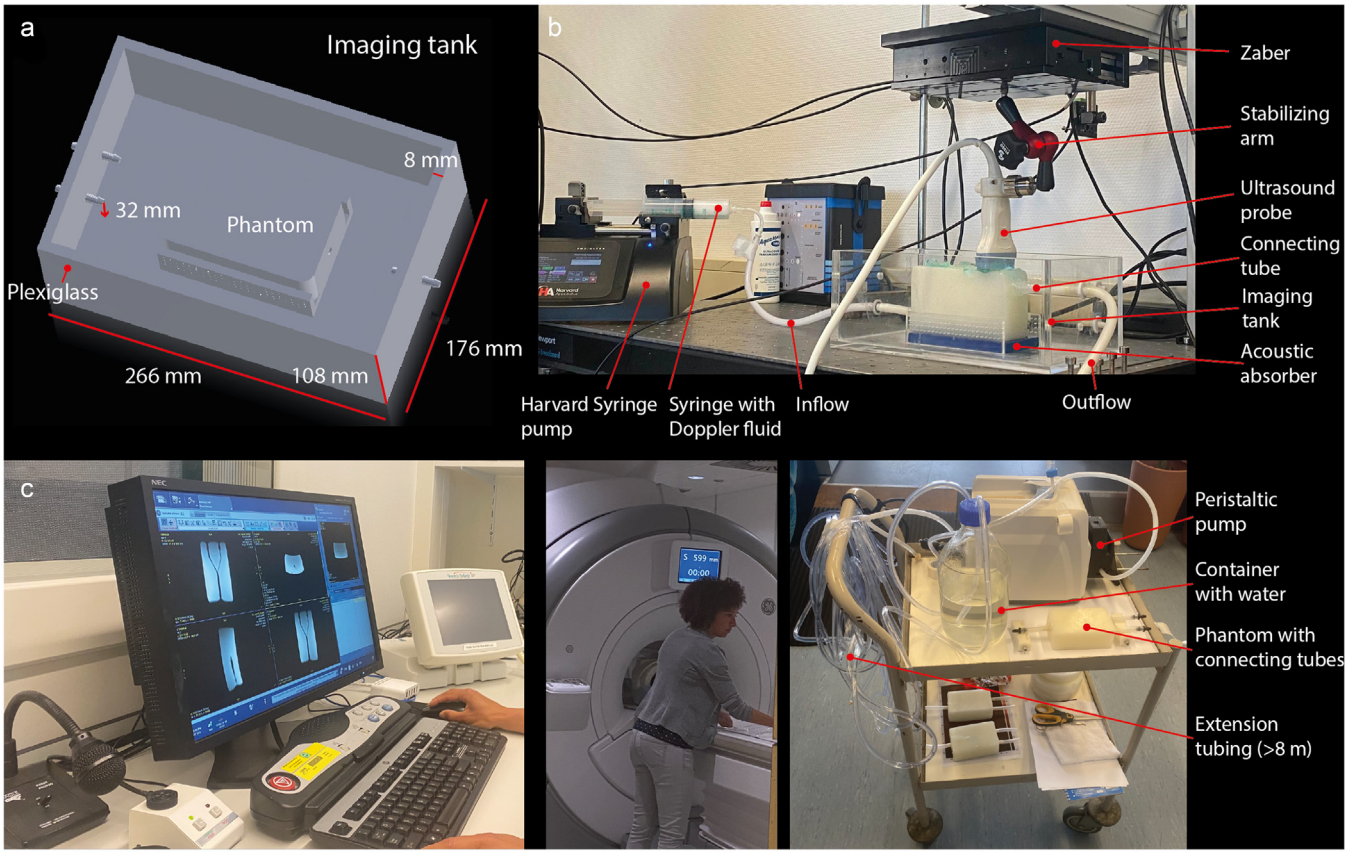

Figure 5. Imaging set-up for (f)US- and MRI-acquisitions. (a) For the ultrasound imaging experiments, as custom tank was designed to allow us to position all phantoms repeatably during imaging. (b) The imaging set-up during one of the Power Doppler measurements of the slanted pipe. In this case, the inflow tract was connected to the syringe pump. In other experiments, the inflow tube was connected to a peristaltic pump. (c) The imaging set-up for the MRI-measurements, which required a significant extension (>8 m) of the in- and outflow tubing.

sequential BFs were filtered using a singular value decomposition (SVD) and summed to form a PDI that was displayed live at a frame rate of 5 Hz. The PDIs as well as the raw data, and angle compounded beamformed frames (BFs) were all stored to a fast PCIe SSD for offline processing purposes.

Speed of sound measurements. First, we assessed the acoustic properties of the phantom tissue mimicking material through speed of sound measurements. The GE9L-D ultrasound transducer was fixated over a homogenous section of each ultrasound phantom, containing only tissue-mimicking material, after which a series of short recordings were performed.

Staged 3D power doppler measurements. Next, we acquired 3D-Doppler volumes of each phantom using a conventional staged acquisition approach. The transducer was mounted to a motorized linear stage motor (X-LDA025A, Zaber Technologies Inc., Vancouver, Canada) (Fig. 4b). Short Doppler recordings of 5 sec each were obtained over the full volume of interest at spatial intervals of 500 μm.

Doppler flow measurements. Finally, we assessed the slanted pipe phantoms Doppler response to different flow rates. For these measurements the probe was stabilized over a sagittal section of the slanted pipe-phantom. The inflow tube was connected to the syringe pump, which was set to a constant infusion rate of either 20, 30, or 40 mL/min. For each flow rate, an ultrasound recording of 30 sec was acquired.

Data processing. Speed of sound measurements. For each speed of sound recording the raw signals were reconstructed using a conventional delay-and-sum approach varying the sound speed in the reconstruction between 1300 and 1700 ms^{-1}. The sharpness of the beamformed images as a function of sound speed were then calculated with a Brenner gradient using the in-built k-Wave toolbox *sharpness* function [28]. The choice of sound speed influences the image focus so quantifying the sharpness in this way allowed for the phantom sound speed to be approximated.

Staged 3D power doppler measurements. For each spatial location, a single PDI was constructed by averaging 150 Singular Value Decomposition (SVD)-filtered beamformed frames. The SVD-threshold to remove the static tissue mimicking components was set heuristically at the first 30 singular components. These PDIs were then concatenated to form a volume and converted to NIfTI format for viewing in 3D Slicer [27] and Paraview (Kitware, Inc.).

Doppler flow measurements. For the different flow rate measurements, the double-sided Doppler spectrum of 5 sec of 1000 Hz filtered beamformed data was reconstructed for each recording by averaging the spectrum over a 2D-ROI inside the phantom. For each spectrum, a moving average filter with a window of 30 samples was passed over it to better highlight the trend between flow rate and obtained Doppler shift.

MRI

Imaging setup. We also assessed the compatibility of our flow phantoms with MRI. To facilitate measurements inside the MRI we were required to significantly extend (>8m) the in- and outflow tubing to avoid placing the peristaltic pump inside the shielded MRI-room. Additionally, for these experiments the tubing was filled with water rather than Doppler fluid.

Data acquisition. MRI was performed at 3T with the phantom placed in either a transmit/receive knee coil (structural images) or a 16-channel head coil (flow images) (Discovery MR750, GE Healthcare, Milwaukee, WI, US). T1-weighted structural scans were acquired with an axial 2D spin echo read-out (voxel size 0.4×0.4×1.2 mm^3, matrix size

256×256×51, repetition time 720 ms, echo time 11 ms, including fat suppression). To quantify T1 and T2 relaxation times of the phantom, a 3D spoiled gradient-recalled echo with multiple flip angles (flip angle: 5, 8, 15 and 22 degrees, voxel size 0.5×0.5×2 mm^3, matrix 256×256×88, repetition time 4.4 ms, echo time 1.9 ms) and multi-echo spin-echo (voxel size 0.6×0.6×3 mm^3, matrix 256×256×32, repetition time 1000 ms, 8 echo times of 6:6:48 ms) were acquired respectively.

To measure flow velocities through the phantoms, phase contrast scans were acquired with bipolar gradients along all three orthogonal directions (velocity encoding of 70 cm/s, repetition time 18 ms, echo time 5 ms, voxel size 0.3×0.3×2.5mm^3, matrix 256×256×18), while the flow was set to a constant 400 revolutions per minute using the previously mentioned peristaltic pump (RPM, equivalent in our set-up to 120 mL/min).

Data processing. T1 calculations were created by fitting the variable flip angle data according to previously reported methods [29]. T2 calculations were done by mono-exponential fitting of the multiecho spin echo data. Both structural T1- and T2-volumes were visualized in Paraview (Kitware, Inc.). The phase contrast scans in three orthogonal directions were reconstructed and used to calculate a weighted image of the flow based on built-in algorithms provided by GE healthcare.

Challenges

Throughout the project, we learnt how to optimize each of the above-mentioned fabrication and imaging steps through trial-and-error. To also document what did *not* work, an overview of all the problems we encountered, including inhomogeneity of the tissue medium, inconsistency of the resin print quality and leakage around the phantom nozzles, are included in Supplementary File 2. Our solutions to each of these problems are also discussed.

Results

Phantom material properties in ultrasound and MRI

Figure 6a shows the sharpness of the reconstructed B-mode image for each phantom as a function of sound speed. The sound speed that generated the highest sharpness, and therefore the most focused B-mode image, was found to be 1470 m/s. The B-mode image reconstructed using the speed of sound corresponding to the highest sharpness is shown in Figure 6b. Reference values for speeds of sound [30] for different soft tissue types are shown in Figure 6c for comparative purposes.

Figure 6d, e show the Y-shape phantom in two orientations for a T1-weighted and T2-weighted MRI scan. For each MRI-sequence, the median value for the relaxation time of the tissue-mimicking material was calculated within a region of interest (white rectangle) and displayed relative to common MRI imaging medium reference values (taken from [31–33]) in Figure 6f.

Volumetric phantom reconstructions in ultrasound and MRI

Figure 7a shows thresholded T1-weighted MRI-reconstructions of each of the three phantoms, with which we were able to visually confirm

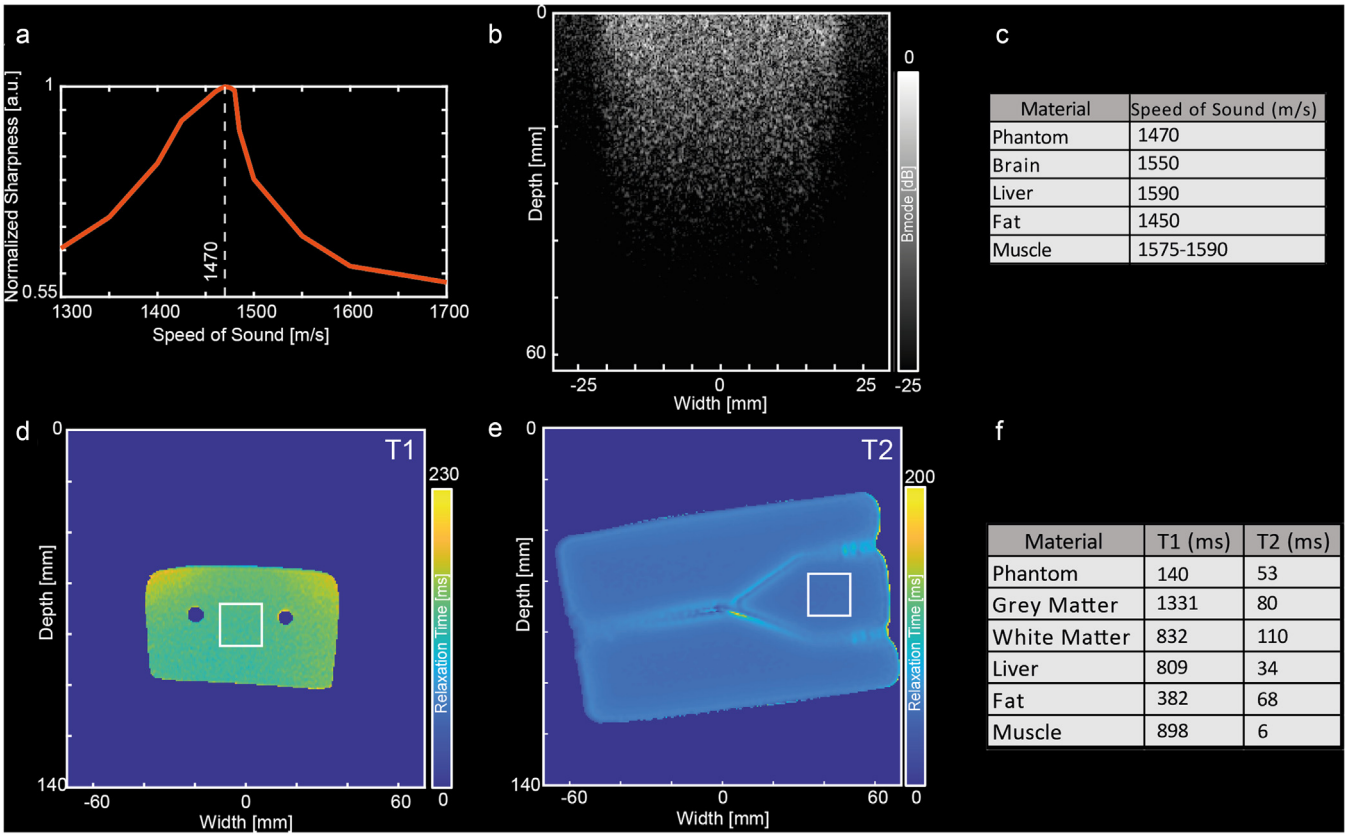

Material	Speed of Sound (m/s)
Phantom	1470
Brain	1550
Liver	1590
Fat	1450
Muscle	1575-1590

Material	T1 (ms)	T2 (ms)
Phantom	140	53
Grey Matter	1331	80
White Matter	832	110
Liver	809	34
Fat	382	68
Muscle	898	6

Figure 6. Structural images: Speed of Sound and MR Relaxation Time. (a) Graph depicting the sharpness of each ultrasound B-mode image obtained for the tested speeds of sound. The speed of sound that allowed for the most focused B-mode image, and therefore the highest sharpness was found to be 1470 m/s. (b) The B-mode image reconstructed using the speed of sound corresponding to the highest sharpness. (c) Reference values for speed of sound in soft tissues, found in [30] for comparative purposes. (d, e) show the Y-shape phantom in two orientations for the quantified T1 and T2 maps resulting from MRI scans. For each image, the median value for the relaxation time of our tissue-mimicking material is calculated within the regions of interest (white rectangle). F) T1- and T2-relaxation times for the phantom displayed relative to common MRI imaging medium reference values (taken from [31–33]).

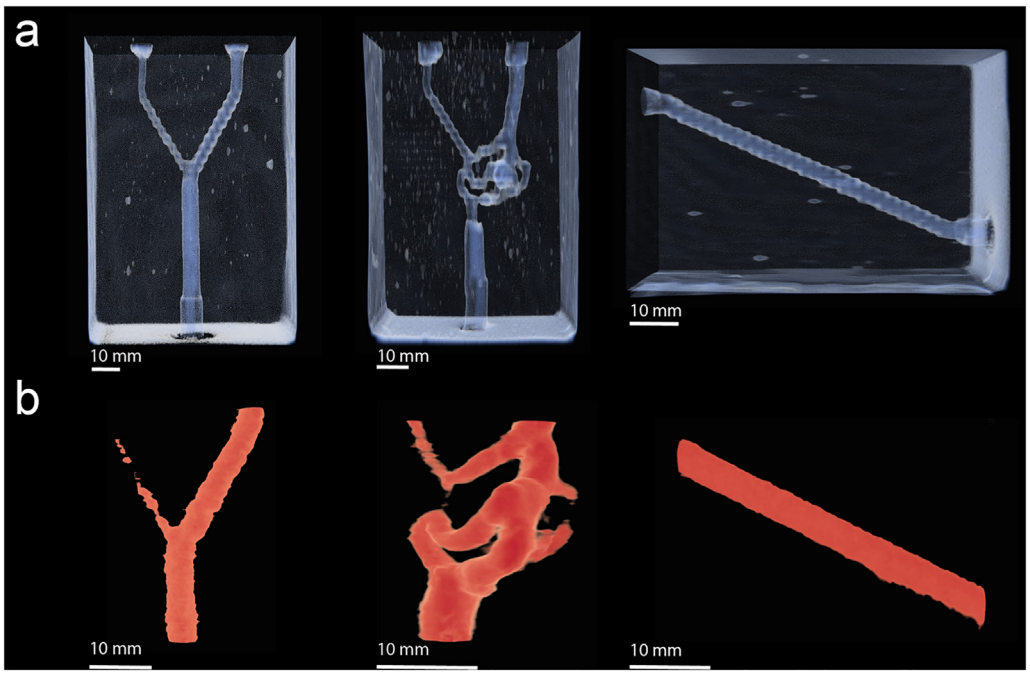

Figure 7. Structural MRI and 3D-PDI reconstructions. (a) Thresholded T1-weighted MRI-reconstructions of our three phantoms, confirming the integrity of the resin-printed cast. (b) 3D-PDI reconstructions of regions of interest for each of these phantoms.

that the resin-print remained intact during the molding process. The thresholded images also reveal small inhomogeneous areas of T1-hyper-intensity inside of the tissue-mimicking material which are most likely pockets of air captured during the phantom pouring process. In Figure 7b we show the 3D-PDI are flow-based reconstructions. These flow reconstructions can demonstrate both the phantom's structural details and that the vascular structure has been nearly fully perfused in each case.

Flow measurements in ultrasound and MRI

Figure 8a shows a PDI obtained while the slanted pipe phantom was connected to the syringe pump, at a constant flow rate of 30 mL/min. Figure 8b shows the double-sided Doppler spectrum of the 1000 Hz filtered beamformed data as reconstructed from the recordings for each flow rate (20, 30, and 40 mL/min). The Doppler spectrum with increasing flow rates shows an increased Doppler shift, as would be expected.

In Figure 9a we show three different axial cross-sections of the MR-phase contrast - flow images of the y-shaped phantom, with Figure 9b indicating from approximately where these cross-sections were evaluated. In Figure 9c an out-of-plane reconstruction of the flow in the bottom part of the y-shape bifurcation (#4).

Storage and durability

As reported by Cabrelli et al. [23], we were able to easily store the phantoms at room temperature without cover. Some of our phantoms were imaged >6 mo after production, without any apparent change in imaging quality.

Discussion

This manuscript describes the manufacturing process of an MRI- and Doppler Ultrasound-compatible flow-phantom using customizable, water-soluble resin prints. As shown in this paper, these resin prints are versatile, allowing for phantom designs ranging from geometrical forms to patient-specific vasculature. We have demonstrated the phantom's

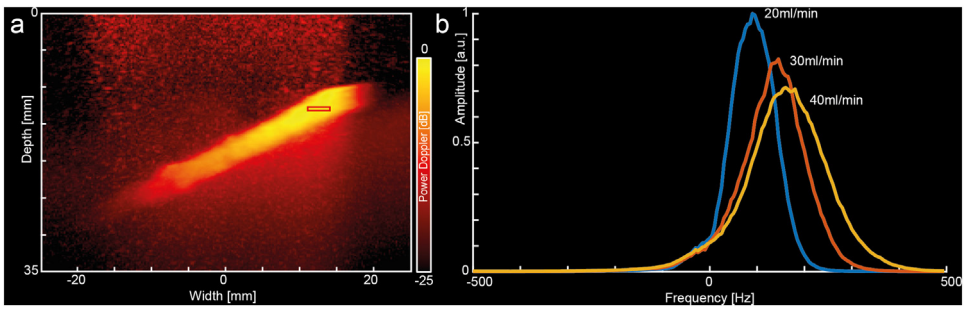

Figure 8. PDI Flow Experiment. (a) PDI obtained while the slanted pipe phantom was connected to the syringe pump, at a constant infusion rate of 30 mL/min. (b) Graph showing the double-sided Doppler spectrum of the 1000 Hz filtered beamformed data as reconstructed for three recordings with increasing flow rates (20, 30, and 40 mL/min) by averaging the spectrum over the region of interest (red ROI in panel A). The Doppler spectrum for each of the increasing flow rates shows a relative Doppler shift, as is to be expected for these flow measurements. PDI, power doppler image, ROI, region of interest.

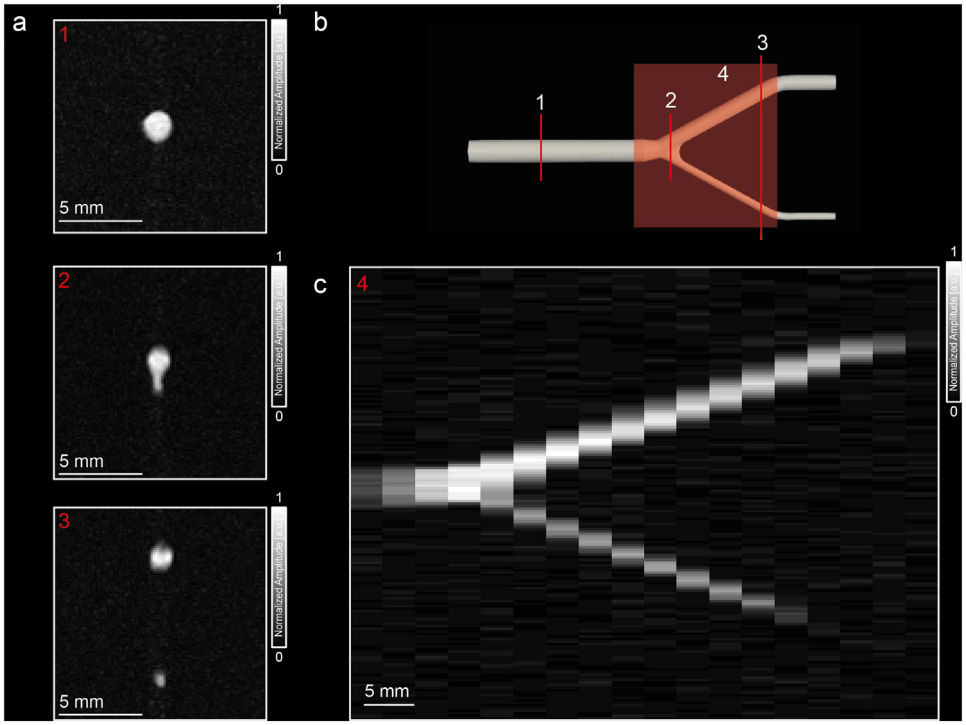

Figure 9. MRI Flow Measurements (Phase Contrast). (a) Flow velocity as calculated in three different axial sections of the y-shape phantom (#1–3) based on Phase Contrast imaging. (b) an out-of-plane reconstruction of the flow velocity in the bottom part of the y-shape bifurcation (#4). In both panels, the maximum flow velocity which was found was around 8 cm/s.

compatibility with both Doppler ultrasound- and MR Phase Contrast-imaging.

Although,

1) The tissue mimicking material used in our phantom has been described before [8,23,34–36]
2) Our soluble resin-material is commercially available (3D-resyn, IM-HDT-WS)
3) Other methods to create wall-less phantoms have been described [37,38],
4) Patient-specific printing of vasculature has also been described [13,17–19,22],

our phantom is unique in that it combines all these aspects to create one single versatile, wall-less ultrasound- and MRI-compatible flow-phantom.

The results in this paper describe the intrinsic acoustic and MRI-properties of our phantom. The speed of sound of our phantom falls in line with the expected speed of sound shown by Cabrelli et al. [23] who measured the same mixture to have a sound speed of 1472 +− 0.6 m/s after >1 y. Despite our streamlining of the phantom pouring pipeline, both air pockets and clusters of TiO_2 were still formed in the tissue mimicking material, as visible in the structural MRI images (Fig. 7a). However, given the relative sparsity of these inhomogeneities (Fig. 7a), they did not noticeably impact the acoustic results.

The phantom design was otherwise favorable in terms of reproducibility and durability. The combination of our phantom mold and imaging unit resulted in a modular set-up, in which different iterations of the same phantom, as well as different phantom types, could be imaged in a consistent, reproducible way. This modular nature, however, also posed constraints. The mold and imaging unit only facilitated a limited number of in- and outflow tracts (max 1–2 on each side). For geometrical shapes, such as the y-shape and slanted pipe, this was not a problem. However, for the patient-specific print, only a limited number of vascular networks would be well-suited for phantom production. Finely vascularized tumor networks with multiple feeding and draining vessels, as we have imaged in the clinic [25], will not fit the current phantom design without simplification of the complex network to only one or two feeding and draining vessels. Additionally, as with most other reported phantoms, our design also does not facilitate any capillary outflow or any type of tissue diffusion.

The resin-printer also constrains the phantom design. Although the printer resolution is exceptionally high (50 μm, as reported by the manufacturer), the printing surface is limited to small shapes of max. 10 cm (see Supplementary File 1). Additionally, despite the printer resolution permitting the accurate realization of many fine vascular networks, we avoided incorporating structures in our prints of <1 mm in diameter. This was done for two reasons: (i) removing such fine resolution structures from the printing plate and preserving their integrity throughout the cleaning and curing process, is challenging and (ii) despite cooling the SEBS-mix prior to pouring, we still found that the heat from the mixture would deform structures <1 mm.

The structural MRI-scans show that the lumen in all phantoms was completely patent. However, the smaller vessels (*e.g.*, in the Y-shape) did not always seem to receive sufficient flow for Doppler imaging, as was seen in Figure 7. This observation could be explained by a combination of the beam-to-flow angle and the lack of flow restriction to the larger vessel. Figures 6, 7 and 9 show the MRI-compatibility of our phantom for both structural and flow imaging. However, our current imaging set-up is not ideal for flow imaging due to the need to extend the in- and outflow tubing (>8 m) to avoid placement of the MRI-incompatible pump in the vicinity of the MRI-scanner. Future effort should focus on using MRI-compatible flow pumps to connect to the phantom. This will also enable the possibility of performing one-to-one comparisons of flow patterns as found in ultrasound versus MRI, which was not possible in the current setting.

Conclusions

We developed a versatile, wall-less MRI-compatible Doppler Ultrasound flow-phantom using customizable, water-soluble resin prints. This paper describes the phantom's manufacturing process, as well as

the phantom's multimodal compatibility with ultrasound and MRI, both structurally and in terms of flow.

Ethical approval

The data presented in this paper include medical images of a single participant planned for neurosurgical AVM-resection. The patient was recruited from the Department of Neurosurgery of Erasmus MC in Rotterdam. Prior to inclusion, written informed consent was obtained in line with the National Medical-Ethical Regulations (MEC-2018-037, NL64082.078.17).

Data availability statement

All data will be made available upon reasonable request to the corresponding author.

Conflict of interest disclosure

The authors have no conflict of interest to declare.

Funding

This work was supported by the NWO-Groot grant of The Dutch Organization for Scientific Research (NWO) (Grant no. 108845), awarded to CUBE (Center for Ultrasound and Brain-Imaging @ Erasmus MC, see for website: www.ultrasoundbrainimaging.com), as well as by the Netherlands Organization for Scientific Research (NWO-ALW 824.02.001; CIDZ), the Dutch Organization for Medical Sciences (ZonMW 91120067; CIDZ), Medical Neuro-Delta (MD 01092019-31082023; CIDZ), and INTENSE LSH-NWO (TTW/00798883; CIDZ).

Acknowledgments

The authors would like to thank Dr. Michael Brown for proofreading the manuscript.

Supplementary materials

Supplementary material associated with this article can be found in the online version at doi:10.1016/j.ultrasmedbio.2024.02.010.

References

[1] Castillo M. Chapter 14: digital subtraction angiography (DSA): basic principles. Vascular imaging of the central nervous system: physical principles, clinical applications, and emerging techniques. Hoboken: John Wiley & Sons; 2013.
[2] Carr JC, Carroll TJ. Magnetic resonance angiography: principles and applications. Magnetic Resonance Angiography: Principles and Applications. New York: Springer; 2012.
[3] Kimura M, Castillo M. Basic principles of computed tomography angiography (CTA). Vascular imaging of the central nervous system: physical principles, clinical applications and emerging techniques. Hoboken: John Wiley & Sons; 2013.
[4] CIRS Technology, Norfolk VU. Model 040 GSE (multi-purpose, multi-tissue US-phantom) and model 069A (Doppler US flow phantom).
[5] Poepping TL, Nikolov HN, Thorne ML, Holdsworth DW. A thin-walled carotid vessel phantom for Doppler ultrasound flow studies. Ultrasound Med Biol 2004;30 (8):1067–78.
[6] Jin Z, Li Y, Yu K, Liu L, Fu J, Yao X, et al. 3D printing of physical organ models: recent developments and challenges. Adv Sci 2021;8:e2101394.
[7] Mehta V, Rath SN. 3D printed microfluidic devices: a review focused on four fundamental manufacturing approaches and implications on the field of healthcare. Bio Design Manuf 2021;4(2):311–43.
[8] Grillo FW, Souza VH, Matsuda RH, Rondinoni C, Pavan TZ, Baffa O, et al. Patient-specific neurosurgical phantom: assessment of visual quality, accuracy, and scaling effects. 3D Print Med 2018;4(1).
[9] Gold Standard Phantoms, Sheffield UK. (QASPER (Quantitative Arterial Spin Labelling Perfusion Reference) phantom.
[10] He Y, Liu Y, Dyer BA, Boone JM, Liu S, Chen T, et al. 3D-printed breast phantom for multi-purpose and multi-modality imaging. Quant Imaging Med Surg 2019;9(1):63–74.
[11] Crasto N, Kirubarajan A, Sussman D. Anthropomorphic brain phantoms for use in MRI systems: a systematic review. Magn Reson Mater Phys Biol Med 2022;35 (2):277–89.
[12] Altermatt A, Santini F, Deligianni X, Magon S, Sprenger T, Kappos L, et al. Design and construction of an innovative brain phantom prototype for MRI. Magn Reson Med 2019;81(2):1165–71.
[13] Coles-Black J, Bolton D, Chuen J. Accessing 3D printed vascular phantoms for procedural simulation. Front Surg 2021;7:626212.
[14] Cogswell PM, Rischall MA, Alexander AE, Dickens HJ, Lanzino G, Morris JM. Intracranial vasculature 3D printing: review of techniques and manufacturing processes to inform clinical practice. 3D Print Med 2020;6(1):18.
[15] Wu Y, Chee AJY, Golzar H, Yu ACH, Tang X. Embedded 3D printing of ultrasound-compatible arterial phantoms with biomimetic elasticity. Adv Funct Mater 2022;32 (25):2110153.
[16] Ommen ML, Schou M, Zhang R, Villagomez Hoyos CA, Jensen JA, Larsen NB, et al. 3D printed flow phantoms with fiducial markers for super-resolution ultrasound imaging. In: Paper presented at: IEEE International Ultrasonics Symposium, IUS; October 22-25, 2018.
[17] Nilsson DPG, Holmgren M, Holmlund P, Wåhlin A, Eklund A, Dahlberg T, et al. Patient-specific brain arteries molded as a flexible phantom model using 3D printed water-soluble resin. Sci Rep 2022;12(1):1–9.
[18] Maneas E, Xia W, Nikitichev DI, Daher B, Manimaran M, Wong RYJ, et al. Anatomically realistic ultrasound phantoms using gel wax with 3D printed moulds. Phys Med Biol 2018;63(1):015033.
[19] Sommer KN, Bhurwani MMS, Tutino V, Siddiqui A, Davies J, Snyder K, et al. Use of patient specific 3D printed neurovascular phantoms to simulate mechanical thrombectomy. 3D Print Med 2021;7(1).
[20] Little CD, Mackle EC, Maneas E, Chong D, Nikitichev D, Constantinou J, et al. A patient-specific multi-modality abdominal aortic aneurysm imaging phantom. Int J Comput Assist Radiol Surg 2022 Sep;17(9):1611–7.
[21] Cetnar AD, Tomov ML, Ning L, Jing B, Theus AS, Kumar A, et al. Patient-specific 3D bioprinted models of developing human heart. Adv Healthc Mater 2021;10(15): e2001169.
[22] Mackle EC, Shapey J, Maneas E, Saeed SR, Bradford R, Ourselin S, et al. Patient-specific polyvinyl alcohol phantom fabrication with ultrasound and x-ray contrast for brain tumor surgery planning. J Vis Exp 2020;2020(161).
[23] Cabrelli LC, Uliana JH, Da Cruz Junior LB, Bachmann L, Carneiro AAO, Pavan TZ. Glycerol-in-SEBS gel as a material to manufacture stable wall-less vascular phantom for ultrasound and photoacoustic imaging. Biomed Phys Eng Express 2021;7(6).
[24] Tanter M, Fink M. Ultrafast imaging in biomedical ultrasound. IEEE Trans Ultrason Ferroelectr Freq Control 2014;61(1):102–19.
[25] Soloukey S, Vincent AJPE, Satoer DD, Mastik F, Smits M, Dirven CMF, et al. Functional ultrasound (fUS) during awake brain surgery: the clinical potential of intra-operative functional and vascular brain mapping. Front Neurosci 2020;13: 1384.
[26] Soloukey S, Verhoef L, van Doormaal PJ, Generowicz BS, Dirven CMF, De Zeeuw CI, et al. High-resolution micro-Doppler imaging during neurosurgical resection of an arteriovenous malformation: illustrative case. J Neurosurg Case Lessons 2022;4(19): CASE22177.
[27] Fedorov A, Beichel R, Kalpathy-Cramer J, Finet J, Fillion-Robin JC, Pujol S, et al. 3D Slicer as an image computing platform for the Quantitative Imaging Network. Magn Reson Imaging 2012;30(9):1323–41.
[28] Treeby BE, Varslot TK, Zhang EZ, Laufer JG, Beard PC. Automatic sound speed selection in photoacoustic image reconstruction using an autofocus approach. J Biomed Opt 2011;16(9):090501.
[29] Deoni SCL. High-resolution T1 mapping of the brain at 3T with driven equilibrium single pulse observation of T1 with high-speed incorporation of RF field inhomogeneities (DESPOT1-HIFI). J Magn Reson Imaging 2007;26(4):1106–11.
[30] Azhari H. Appendix A: Typical acoustic properties of tissues. Basics of Biomedical Ultrasound for Engineers. Hoboken: John Wiley & Sons; 2010. p. 313–4.
[31] Wansapura JP, Holland SK, Dunn RS, Ball WS. NMR relaxation times in the human brain at 3.0 Tesla. J Magn Reson Imaging 1999;9(4):531–8.
[32] De Bazelaire CMJ, Duhamel GD, Rofsky NM, Alsop DC. MR imaging relaxation times of abdominal and pelvic tissues measured in vivo at 3.0 T: preliminary results. Radiology 2004;230(3):652–9.
[33] Bojorquez JZ, Bricq S, Acquitter C, Brunotte F, Walker PM, Lalande A. What are normal relaxation times of tissues at 3 T? Magn Reson Imaging 2017;35:69–80.
[34] Wang Y, Agyekum EA, Chen J, Du J, Ren Y, Zhang Q, et al. Fabrication of SEBS block copolymer-based ultrasound phantom containing mimic tumors for ultrasound-guided needle biopsy training. Ultrasound Med Biol 2022;48(6):1143–50.
[35] Cabrelli LC, Pelissari PIBGB, Deana AM, Carneiro AAO, Pavan TZ. Stable phantom materials for ultrasound and optical imaging. Phys Med Biol. 2017;62(2):432–47.
[36] Cabrelli LC, Grillo FW, Sampaio DRT, Carneiro AAO, Pavan TZ. Acoustic and elastic properties of glycerol in oil-based gel phantoms. Ultrasound Med Biol. 2017;43 (9):2086–94.
[37] Nikitichev DI, Barburas A, McPherson K, Mari JM, West SJ, Desjardins AE. Construction of 3-dimensional printed ultrasound phantoms with wall-less vessels. J Ultrasound Med. 2016;35(6):1333–9.
[38] Ho CK, Chee AJY, Yiu BYS, Tsang ACO, Chow KW, Yu ACH. Wall-less flow phantoms with tortuous vascular geometries: design principles and a patient-specific model fabrication example. IEEE Trans Ultrason Ferroelectr Freq Control 2017;64(1):25–38.